

July 20, 2021

PREPARED FOR SUBMISSION TO JHEP

N³LO gravitational spin-orbit coupling at order G^4

Michèle Levi,^{a,b} Andrew J. McLeod,^a and Matthew von Hippel^a

^a*Niels Bohr International Academy, Niels Bohr Institute, University of Copenhagen,
Blegdamsvej 17, 2100 Copenhagen, Denmark*

^b*Institut de Physique Théorique, CEA & CNRS, Université Paris-Saclay,
91191 Gif-sur-Yvette, France*

E-mail: michelelevi@nbi.ku.dk, amcleod@nbi.ku.dk, mvonhippel@nbi.ku.dk

ABSTRACT: In this paper we derive for the first time the N³LO gravitational spin-orbit coupling at order G^4 in the post-Newtonian (PN) approximation within the effective field theory (EFT) of gravitating spinning objects. This represents the first computation in a spinning sector involving three-loop integration. We provide a comprehensive account of the topologies in the worldline picture for the computation at order G^4 . Our computation makes use of the publicly-available `EFTofPNG` code, which is extended using loop-integration techniques from particle amplitudes. We provide the results for each of the Feynman diagrams in this sector. The three-loop graphs in the worldline picture give rise to new features in the spinning sector, including divergent terms and logarithms from dimensional regularization, as well as transcendental numbers, all of which survive in the final result of the topologies at this order. This result enters at the 4.5PN order for maximally-rotating compact objects, and together with previous work in this line, paves the way for the completion of this PN accuracy.

Contents

1	Introduction	1
2	EFT of gravitating spinning objects	3
3	Diagrammatic expansion	6
3.1	Topologies	7
3.2	Graphs	11
3.3	Integration and scalability	11
3.4	Findings	12
4	N³LO gravitational spin-orbit action at G^4	14
5	Conclusions	14

1 Introduction

The recent detection of gravitational waves (GWs) by the LIGO collaboration [1, 2] has reinforced the importance and urgency of high-precision gravity predictions. The world-wide network of ground-based detectors has been continually growing [3, 4] with upcoming ground- and space-based detectors to reach a broader band of frequencies, as well as higher sensitivities [5–9]. These observations are primarily designed to detect the mergers of binaries of compact components, which build up to this dramatic event via a long inspiral phase in which they orbit each other with non-relativistic velocities. For this reason the analytical study of the post-Newtonian (PN) approximation of General Relativity has become crucial, including the orbital dynamics of the compact binaries [10], an essential ingredient for the theoretical waveform models that are created using the effective one-body (EOB) framework [11].

Table 1 shows the complete state of the art in PN orbital dynamics of generic compact binaries to date. Each correction enters at the $n + l + \text{Parity}(l)/2$ -th PN order, where n indicates the N ^{n} LO, l indicates the order in spin up to the l -th multipole S^l , and the parity is 0 or 1 for even or odd l , respectively. The table lists the number of the highest-loop graphs (as defined in section 3.1 below) in each sector as a measure of its computational scale in the effective field theory (EFT) framework for PN gravity [12, 13], with n loops entering generically at N ^{n} LO. Note that, in the non-spinning sector, when the Kaluza-Klein (KK) field decomposition [14, 15] is employed, only the $2\lfloor n/2 \rfloor$ -loop level is required, such that e.g., at the 5PN order only the four-loop level is relevant, and so the entry on the first row at N⁵LO is 0 [13]. All sectors up to the 4PN order (apart from the top right one in the non-spinning sector) are available within the public EFTofPNG code [16, 17].

$\begin{smallmatrix} n \\ l \end{smallmatrix}$	$(N^0)\text{LO}$	$N^{(1)}\text{LO}$	$N^2\text{LO}$	$N^3\text{LO}$	$N^4\text{LO}$	$N^5\text{LO}$
S^0	1	0	3	0	25	0
S^1	2	7	32	174		
S^2	2	2	18	52		
S^3	4	24				
S^4	3	5				

Table 1. The number of highest-loop graphs in the worldline picture contributing to each sector in the state-of-the-art of PN gravity for the orbital dynamics of compact binaries.

So far the sectors with boldface entries in table 1 have been completed for generic compact binaries only via the EFT formulation of gravitating spinning objects introduced in [18], see [19–24]. The formulation in [18], which also provided the leading gravitational couplings to all orders in spin, thus enabled the completion of the current state of the art to the 4PN order. The work in [18] was also recently extended to the NLO of the cubic- and quartic-in-spin sector at the 4.5 and 5PN orders [22, 24], which are to date the only PN works to explore the gray area in table 1. The latter is associated with the gravitational Compton scattering with spins $s \geq 3/2$, as classical effects with spin to the l -th order correspond to amplitudes involving a quantum spin of $s = l/2$ [25].

In this work, we derive for the first time via the EFT of spinning gravitating objects the $N^3\text{LO}$ spin-orbit coupling from interaction at G^4 , which consists of the highest-loop graphs in this sector at three-loop level. This is the highest loop level tackled in the spinning sector so far. This coupling enters at the 4.5PN order for maximally-rotating compact objects, and together with the sector tackled in [22], this sector completes the accuracy at 4.5PN order, thus uniquely pushing the precision frontier of PN gravity via the EFT of spinning gravitating objects. This work follows the EFT approach from [12], building on the EFT of gravitating spinning objects [18] and its implementation in the unique public **EFTofPNG** code in [16, 17], to exploit more methods from particle amplitudes. This work also builds on the implementations of [18] at the two-loop level in [20, 21, 26–28], and on prior work at the $N^3\text{LO}$ in the non-spinning sector in [29–37]. Possible tails of radiation reaction involving spin couplings enter at the 5.5PN order [10, 38], namely beyond the order considered in the current sector, so no IR divergences are involved in this work.

Beyond the conceptual difficulty of tackling spins in gravity, the spinning sectors are also rather challenging at the computational level. It was already highlighted in [22] that sectors that have an even order in the spin (in particular also the non-spinning sector) are consistently easier to handle than those which are odd. First, at this loop order it is known that simple poles and their accompanying logarithms in dimensional regularization arise at G^4 also with traditional PN methods [10]. Yet, in the non-spinning sector in an EFT computation with the KK decomposition of the metric, such intricate features do not show up at G^4 [36, 37], since as was noted above the KK decomposition postpones the appearance of three-loop integration to the $N^4\text{LO}$. Thus, while there are no graphs that

enter at three-loop level at the $N^3\text{LO}$ without spins, in the spin-orbit sector there are 174 such graphs, as shown in table 1.

This sector is also more complex in terms of raw number of graphs with 388 graphs to evaluate, compared to only 8 in the $N^3\text{LO}$ non-spinning sector. This is because in contrast to the non-spinning case, in the spinning sectors all possible topologies are realized at each order of G [39]. Second, since spins are derivatively coupled, we tackle integrand tensor numerators as high as rank eight, comparable to $N^5\text{LO}$ in the non-spinning sector. Further, this derivative coupling introduces more time derivatives due to the spin couplings. Finally, and related to the previous point, another notable aspect that further demonstrates the relative intricacy of the spinning sectors with respect to the non-spinning ones is that accelerations enter already at the LO spin-orbit sector [40], that is at the 1.5PN order, compared to the $N^2\text{LO}$ in the non-spinning sector which is at the 2PN order.

This paper is organized as follows. We begin in section 2 by presenting the formal setup within the EFT of gravitating spinning objects. We then proceed in section 3 to study the diagrammatic expansion, first looking into the new topologies in the present spinning sector by revisiting the structure of topologies in the EFT approach from the ground up in section 3.1. We go on to consider the specific graphs that need to be evaluated in this sector in section 3.2, and evaluate them by supplementing the `EFTofPNG` code with common methods from particle amplitudes, in section 3.3. We then discuss the findings of our evaluations, highlighting some special features in section 3.4, and discuss the total outcome for the sector in section 4. Finally, we conclude in section 5.

2 EFT of gravitating spinning objects

We first present the formal setup required to carry out the EFT computation of the $N^3\text{LO}$ spin-orbit sector at order G^4 . Here we will build on the presentation in [28] and [13] (as well as the references therein), reviewing the relevant part of the one-particle effective action, and introducing the new Feynman rules that enter at this order. Note, though, that we will keep here all dependence on the number of spatial dimensions, d , explicit, as done in the `EFTofPNG` code [16], due to our use of dimensional regularization (with the appearance of related divergences, as shall be seen in section 3).

Let us recall the two-particle effective action describing a compact binary system [12, 13], which reads

$$S_{\text{eff}} = S_g[g_{\mu\nu}] + \sum_{a=1}^2 S_{\text{pp}}(\lambda_a), \quad (2.1)$$

where S_g is the pure gravitational action, and S_{pp} is the worldline point-particle action for each of the two components of the binary, which depends on a worldline parameter of the a -th component, λ_a .

First, we need to take into account the purely gravitational action at the orbital scale. This is given in terms of the gravitational field, $g_{\mu\nu}(x)$, as follows:

$$S_g[g_{\mu\nu}] = S_{\text{EH}} + S_{\text{GF}} = -\frac{1}{16\pi G_d} \int d^{d+1}x \sqrt{g} R + \frac{1}{32\pi G_d} \int d^{d+1}x \sqrt{g} g_{\mu\nu} \Gamma^\mu \Gamma^\nu, \quad (2.2)$$

where $\Gamma^\mu \equiv \Gamma_{\rho\sigma}^\mu g^{\rho\sigma}$, and we have the Einstein-Hilbert action supplemented by a gauge-fixing term, chosen to be the fully harmonic gauge. Note that, similar to the modified minimal subtraction ($\overline{\text{MS}}$) prescription [41], we use here the generic d -dimensional gravitational constant, G_d , defined as:

$$G_d \equiv G_N \left(\sqrt{4\pi e^\gamma} R_0 \right)^{d-3}, \quad (2.3)$$

where $G_N \equiv G$ is Newton's gravitational constant in three-dimensional space, γ is Euler's constant, and R_0 is a fixed renormalization scale. In what follows, we will use $\epsilon \equiv d - 3$ to denote the dimensional parameter in dimensional regularization.

We then decompose the gravitational field into a $d+1$ non-relativistic form in a Kaluza-Klein (KK) fashion:

$$ds^2 = g_{\mu\nu} dx^\mu dx^\nu \equiv e^{2\phi} (dt - A_i dx^i)^2 - e^{-\frac{2}{d-2}\phi} \gamma_{ij} dx^i dx^j. \quad (2.4)$$

This parametrization has considerably facilitated higher-order PN computations in the EFT approach [14, 15]. Eq. (2.4) defines the KK fields: ϕ , A_i , and $\gamma_{ij} \equiv \delta_{ij} + \sigma_{ij}$, identified as the Newtonian scalar, the gravito-magnetic vector, and the symmetric tensor, respectively. The gravitational action in eq. (2.2) is worked out in terms of the KK fields in [42], and in more detail in the **EFTofPNG** code [16]. This action gives rise to the following propagators for the KK fields:

$$\langle \phi(x_1) \phi(x_2) \rangle = \text{---} = \frac{16\pi G_d}{c_d} \cdot \delta(t_1 - t_2) \int_{\vec{k}} \frac{e^{i\vec{k} \cdot (\vec{x}_1 - \vec{x}_2)}}{\vec{k}^2}, \quad (2.5)$$

$$\langle A_i(x_1) A_j(x_2) \rangle = \text{---} = -16\pi G_d \cdot \delta(t_1 - t_2) \int_{\vec{k}} \frac{e^{i\vec{k} \cdot (\vec{x}_1 - \vec{x}_2)}}{\vec{k}^2} \delta_{ij}, \quad (2.6)$$

$$\langle \sigma_{ij}(x_1) \sigma_{kl}(x_2) \rangle = \text{=} = 32\pi G_d \cdot \delta(t_1 - t_2) \int_{\vec{k}} \frac{e^{i\vec{k} \cdot (\vec{x}_1 - \vec{x}_2)}}{\vec{k}^2} P_{ij;kl}, \quad (2.7)$$

where we abbreviate $\int \frac{d^d \vec{k}}{(2\pi)^d}$ as $\int_{\vec{k}}$, $P_{ij;kl} \equiv \frac{1}{2}(\delta_{ik}\delta_{jl} + \delta_{il}\delta_{jk} + (2 - c_d)\delta_{ij}\delta_{kl})$, and $c_d \equiv 2(d - 1)/(d - 2)$. These propagators receive perturbative relativistic corrections from quadratic vertices involving two time derivatives; however, since we only consider the leading contribution in G^4 to the N³LO sector in this paper such corrections will not play a role.

Let us turn now to the Feynman rules required for this sector, which go beyond those appearing in the lower-order spinning sectors, presented in [28]. The latter can be found for generic d in the public **EFTofPNG** code [16]. The Feynman rules relevant as of this order were also obtained by extending the **FeynRu1** module of the **EFTofPNG** code [16].

We consider first the bulk vertices. There are two new cubic self-interaction vertices to consider,

$$\begin{aligned} \text{---} &= \frac{1}{256\pi G_d} \int d^{d+1}x \left[\sigma_{ii} [(\partial_i \sigma_{jj})^2 - 2(\partial_i \sigma_{jk})^2 + 4(\partial_i \sigma_{ij})^2 - 4\partial_i \sigma_{jk} \partial_j \sigma_{ik}] \right. \\ &\quad \left. + 2[4\sigma_{ij} \partial_k \sigma_{ik} - 4\sigma_{ik} \partial_i \sigma_{jk} - 2\sigma_{ik} \partial_j \sigma_{ik} - \sigma_{ij} \partial_i \sigma_{kk}] \partial_j \sigma_{ii} \right] \end{aligned}$$

$$+ 4\sigma_{ij} [\partial_i \sigma_{kl} \partial_j \sigma_{kl} - 2\partial_k \sigma_{ik} \partial_l \sigma_{jl} + 2\partial_k \sigma_{il} \partial_k \sigma_{jl} + 2\partial_k \sigma_{il} \partial_l \sigma_{jk}] \Big], \quad (2.8)$$

$$\begin{aligned} \text{---} \text{---} \text{---} \text{---} &= \frac{1}{64\pi G_d} \int d^{d+1}x \Big[[\partial_i A_i \partial_t \sigma_{jj} - \partial_t A_i \partial_i \sigma_{jj} + 2\partial_t A_i \partial_j \sigma_{ij} - 2\partial_i A_j \partial_t \sigma_{ij}] \sigma_{ii} \\ &+ A_i [\partial_t \sigma_{jj} (\partial_i \sigma_{kk} - 2\partial_k \sigma_{ik}) + 2\partial_t \sigma_{ij} (\partial_j \sigma_{kk} - 2\partial_k \sigma_{jk}) - 2\partial_t \sigma_{jk} (\partial_i \sigma_{jk} - 2\partial_j \sigma_{ik})] \\ &+ 2\partial_t A_i [\sigma_{ij} (\partial_j \sigma_{kk} - 2\partial_k \sigma_{jk}) + \sigma_{jk} (\partial_i \sigma_{jk} - 2\partial_j \sigma_{ik})] \\ &- 2\partial_j A_i [\sigma_{ij} \partial_t \sigma_{kk} - 2\sigma_{ik} \partial_t \sigma_{jk} - 2\sigma_{jk} \partial_t \sigma_{ik}] - 2\partial_i A_i \sigma_{jk} \partial_t \sigma_{jk} \Big], \end{aligned} \quad (2.9)$$

three new quartic self-interaction vertices,

$$\begin{aligned} \text{---} \text{---} \text{---} \text{---} &= \frac{c_d}{64\pi G_d} \int d^{d+1}x \Big[\phi \Big[\sigma_{ii} \Big(\partial_i A_j (\partial_i A_j - \partial_j A_i) + (\partial_i A_i)^2 \Big) \\ &+ 2\sigma_{ij} \Big[2(\partial_i A_k \partial_k A_j - \partial_i A_j \partial_k A_k) - (\partial_i A_k \partial_j A_k + \partial_k A_i \partial_k A_j) \Big] \Big], \end{aligned} \quad (2.10)$$

$$\text{---} \text{---} \text{---} \text{---} = \frac{c_d}{32\pi G_d} \int d^{d+1}x \Big[(2\sigma_{ij} A_i \partial_j \phi - \sigma_{ii} A_j \partial_j \phi) \partial_t \phi \Big], \quad (2.11)$$

$$\begin{aligned} \text{---} \text{---} \text{---} \text{---} &= \frac{c_d}{256\pi G_d} \int d^{d+1}x \Big[(\partial_i \phi)^2 (2(\sigma_{ij})^2 - (\sigma_{ii})^2) \\ &+ 4\partial_i \phi \partial_j \phi (\sigma_{kk} \sigma_{ij} - 2\sigma_{ik} \sigma_{jk}) \Big], \end{aligned} \quad (2.12)$$

and one new quintic self-interaction vertex,

$$\text{---} \text{---} \text{---} \text{---} \text{---} = \frac{c_d^3}{192\pi G_d} \int d^{d+1}x \phi^3 \Big(\partial_i A_j (\partial_i A_j - \partial_j A_i) + (\partial_i A_i)^2 \Big). \quad (2.13)$$

Notice that at this order the KK tensor field σ_{ij} starts to play an important role in the interaction, and that all these vertices contain at most a single time derivative.

Let us proceed then to consider the point-particle action of a spinning particle [13]. Since we are considering the spin-orbit sector, which is linear in the spins of the particles, it is sufficient here to take into account only the minimal coupling part of the effective action of each of the spinning particles. This part of the action reads [18]:

$$S_{\text{pp}}(\lambda) = \int d\lambda \left[-m\sqrt{u^2} - \frac{1}{2} \hat{S}_{\mu\nu} \hat{\Omega}^{\mu\nu} - \frac{\hat{S}^{\mu\nu} p_\nu}{p^2} \frac{Dp_\mu}{D\lambda} \right], \quad (2.14)$$

where m is the mass, u^μ is the 4-velocity, p_μ is the conjugate linear momentum, and $\hat{\Omega}^{\mu\nu}$ and $\hat{S}_{\mu\nu}$, are the generic angular velocity and spin variables of the particle, respectively. This form of the action in eq. (2.14) is covariant, as well as invariant under gauge of the rotational variables [18]. This is in contrast to the action presented in [43–45], which does not have generic rotational variables, and does not include the last term in eq. (2.14). Note that both the mass and spin couplings play important roles in the spin-orbit interaction.

Additional worldline mass couplings are also required at N³LO. In particular, we have the following two new Feynman rules for four-graviton couplings:

$$\begin{array}{c} \bullet \\ \text{---} \end{array} \begin{array}{c} \diagup \\ \diagdown \\ \diagup \\ \diagdown \end{array} = -\frac{1}{24}m \int dt \phi^4, \quad (2.15)$$

$$\begin{array}{c} \bullet \\ \text{---} \end{array} \begin{array}{c} \diagup \\ \diagdown \\ \text{---} \\ \text{---} \end{array} = \frac{1}{6}m \int dt \phi^3 A_i v^i, \quad (2.16)$$

where the thick vertical lines represent worldlines, and the spherical blobs represent mass insertions.

Finally, let us consider the new worldline spin couplings required in this sector. For the two-graviton coupling to the worldline spin, the new Feynman rule is

$$\begin{array}{c} \text{---} \\ \text{---} \end{array} \text{---} \text{---} = \frac{1}{8} \int dt [S_{ij}\sigma_{il} [2v^m (\partial_j \sigma_{lm} - \partial_l \sigma_{jm}) + v^m \partial_m \sigma_{jl} + \partial_t \sigma_{jl}]], \quad (2.17)$$

where the oval blobs stand for the spin dipole sources. Notice in particular the last term, which involves a time derivative, that enters here at the LO of the vertex; This did not occur in vertices at lower orders. These rules are already given in terms of the physical spatial components of the local spin tensor in the canonical gauge [18], so all indices are Euclidean. For the three-graviton coupling to the worldline spin, the new Feynman rule is

$$\begin{array}{c} \text{---} \\ \text{---} \end{array} \text{---} \text{---} = \frac{c_d}{4} \int dt [S_{ij}\sigma_{il} (\partial_j A_l - \partial_l A_j) \phi], \quad (2.18)$$

and for the four-graviton coupling to the worldline spin, the new Feynman rule is

$$\begin{array}{c} \text{---} \\ \text{---} \end{array} \text{---} \text{---} = \frac{c_d^3}{12} \int dt [S_{ij}\partial_i A_j \phi^3]. \quad (2.19)$$

Note that similar to what happens as of the NLO, at the NⁿLO, the (n+1)-scalar graviton-spin coupling is absent in the KK fields together with our gauge choice for the rotational variables. Thus, this vertex is deferred to higher PN orders.

3 Diagrammatic expansion

In this section we present and evaluate the Feynman diagrams that comprise the perturbative PN expansion of the N³LO spin-orbit sector at order G^4 . As illustrated in table 1, the analysis of this sector builds on the N²LO spin-orbit sector obtained in [46–48], and in [28] via the EFT of spinning gravitating objects, and on the non-spinning N³LO sector (at the 3PN order) [29–37]. In contrast to the non-spinning case, all possible topologies are



Figure 1. The single graph topology at order G : One-graviton exchange with no self-interaction.

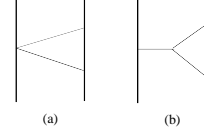


Figure 2. Graph topologies at order G^2 : (a) No self-interaction vertices. (b) One cubic vertex. This is a one-loop topology in the worldline picture.

realized in the spinning sector at each order of G [39]. Hence, in the present sector three-loop topologies (in the worldline picture, as specified below) must be tackled, including topologies whose integrals need to be reduced using integration by parts (IBP) [49]. This is unlike the situation in the non-spinning sector, where such three-loop topologies appear only at N⁴LO (at the 4PN order) [13].

We start by giving a comprehensive account of the topologies and the corresponding integrals that appear in this sector, before proceeding to enumerate all of the Feynman graphs and their evaluation. Similar to the ingredients presented in the previous section, all of the computational aspects of the work presented in this section were carried out using the `EFTofPNG` code [16, 17], that has been extended to handle this challenging sector.

3.1 Topologies

Let us begin by describing the generic topologies that enter at order G^4 . To establish our terminology, we first review the topologies that appear at lower orders of G ; these are shown for G^1 , G^2 , and G^3 in figures 1, 2, 3, respectively [13].

First we consider the integral expressions which correspond to the various topologies. For instance, graph (a) in figure 2 is proportional to

$$\text{Fig. 2(a)} \sim \int_{\vec{p}_1} \frac{e^{i\vec{p}_1 \cdot (\vec{x}_1 - \vec{x}_2)}}{\vec{p}_1^2} \int_{\vec{p}_2} \frac{e^{i\vec{p}_2 \cdot (\vec{x}_1 - \vec{x}_2)}}{\vec{p}_2^2}, \quad (3.1)$$

so this is just a factorization into two copies of the basic topology at order G shown in figure 1. However, if we perform the following simple change of variables:

$$p_1 + p_2 \rightarrow p, \quad p_2 \rightarrow k_1, \quad (3.2)$$

we obtain

$$\text{Fig. 2(a)} \rightarrow \int_{\vec{p}} e^{i\vec{p} \cdot (\vec{x}_1 - \vec{x}_2)} \int_{\vec{k}_1} \frac{1}{\vec{k}_1^2 (\vec{p} - \vec{k}_1)^2} \sim \text{Fig. 2(b)}, \quad (3.3)$$

where p is the Fourier momentum (or the momentum transfer of the source), and k_1 is the loop momentum. Hence, we see that both topologies at order G^2 can also be expressed in terms of a single basic one-loop integral. On the other hand, from eq. (3.1) which is written directly in the worldline picture, we see that the topologies that appear at each higher order in G are often no more complicated than those appearing at lower orders. It is thus beneficial to discern the worldline picture, in which all topologies and graphs in this

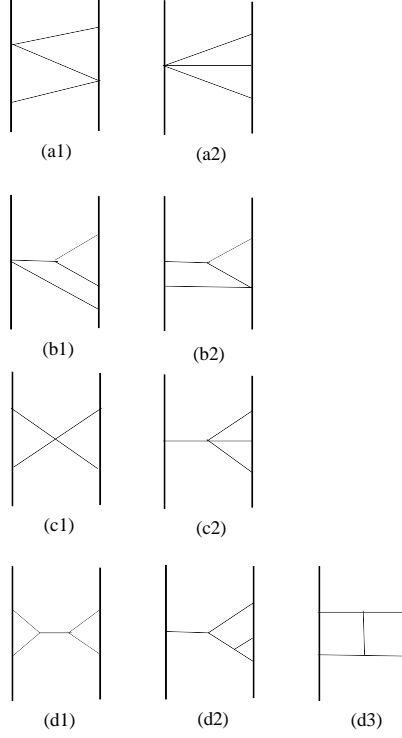


Figure 3. Graph topologies at order G^3 : (a) No self-interaction vertices. (b) One cubic vertex. (c) One quartic vertex. (d) Two cubic vertices. Topologies (c) and (d) constitute two-loop topologies in the worldline picture. The topology (d3) is a rank-two topology as specified below.

paper are drawn. This is facilitated by considering the following useful definition of loop order in the worldline picture, which we will use to classify all graphs in this paper:

Definition 1 *The loop order, n_L , of a graph at order G^n in the worldline picture can be defined as*

$$n_L \equiv 2n - \sum_{i=1}^{n+1} m_i, \quad (3.4)$$

where m_i denote the numbers of gravitons in each of the $n + 1$ worldline insertions.

In particular, we see that the maximal loop order in the worldline picture at order G^n , which is $n - 1$, is realized only in the topologies which contain exclusively one-graviton worldline insertions. For instance, figure 2(b) is a one-loop topology, whereas the factorizable figure 2(a) is a 0-loop topology.

It is straightforward to generalize the change of variables in eq. (3.2), as well as to apply the definition above to topologies at higher orders in G . This gives us two possible perspectives on any given graph at order G^{n+1} : either in a form standardized into a n -loop integral, using a change of variables as in eq. (3.2), which corresponds to the quantum picture of a two-point function with massless propagators [13, 50]; or in the worldline picture, with integrals that may factorize into a product with copies of the basic 0-loop

topology at order G . In particular, graphs with m -graviton worldline insertions, where $m \geq 2$, are always factorized in this way and correspond to lower-loop graphs in the worldline picture.

With these two perspectives in mind, the topologies at order G^3 (shown in figure 3) can be classified into three types according to their two-loop standardized integral form, as detailed in [26]:

1. The *nested* type, which includes most of the topologies at this order, $\{(a1), (a2), (b1), (b2), (c2), (d2)\}$.
2. The *factorizable* type, which includes only the two topologies $\{(c1), (d1)\}$.
3. The topologies that are neither of the two former types, which must be reduced to a linear combination of the two former basic integrals using IBP relations. Only topology (d3) falls into this class.

In view of the above classification it is useful to introduce the following definition:

Definition 2 *We define a topology at order G^{n+1} to be of rank r , when r of the basic n -loop integral types are required in order to express its n -loop integral form.*

For instance, topology (d3) is a rank-two topology since it is expressed in terms of linear combinations of (the integrals corresponding to) nested and factorizable topologies. All other topologies at this order are rank-one topologies, since they are themselves nested or factorizable.

Let us finally proceed to the topologies that appear in the spin-orbit sector at order G^4 , which are shown in figure 4. There are in fact three basic types of integrals, which form a basis for the topologies at this order. The 32 topologies at this order can be classified as follows:

1. The *nested-nested* type, which accounts for 22 of the topologies, $\{(a), (b), (c2)-(c3), (d2), (e1)-(e3), (e5)-(e7), (f3)-(f4), (g2)-(g3)\}$.
2. The *factorizable-nested* type, which includes topologies $\{(d1), (f1), (f2), (g1)\}$.
3. The *nested-factorizable* type, which includes only the topologies $\{(c1), (e4)\}$. This type cannot be realized as a three-loop topology in the worldline picture, where it actually contains only two-loop topologies. Any attempt to draw such a three-loop graph would contain graviton loops, which are purely quantum, and excluded in our setup. Of course, this type is still three-loop in the quantum two-point function picture [51].
4. Beyond these basic types, there are higher-rank topologies, which can be further subdivided:
 - (a) There is a single rank-two type, which can be expressed as a combination of the nested-nested and the nested-factorizable topologies. There is a single topology of this type, (e8).

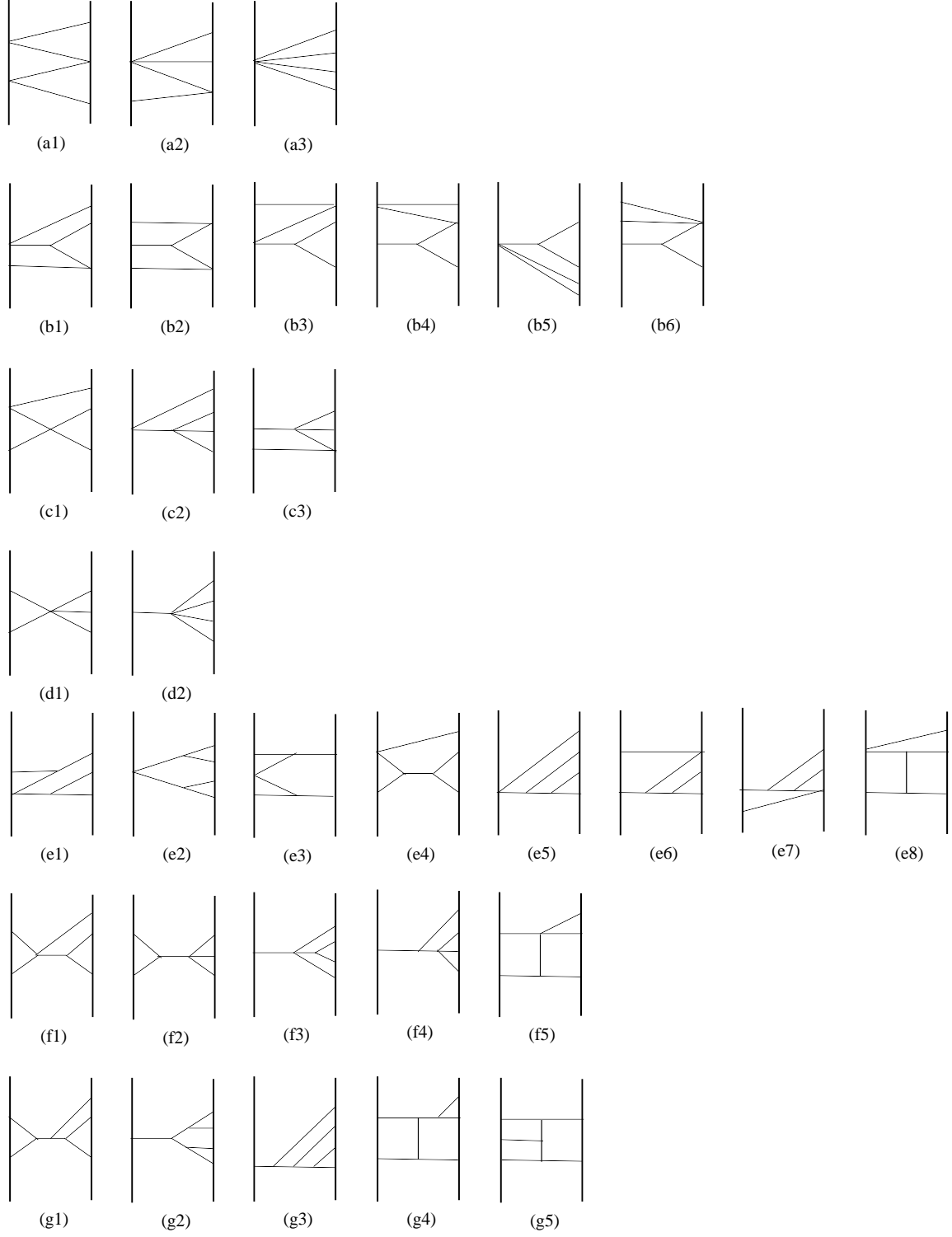


Figure 4. Graph topologies at order G^4 : (a) No self-interaction vertices. (b) One cubic vertex. (c) One quartic vertex. (d) One quintic vertex. (e) Two cubic vertices. (f) One cubic vertex and one quartic vertex. (g) Three cubic vertices.

- (b) The rank-three topologies, $\{(f5), (g4), (g5)\}$, which can only be expressed in terms of linear combinations of all three basic integral types at this order.

The rank-one topologies all boil down to one-loop computations, whereas higher-rank topologies need to be worked out more laboriously. Notice that only 12 topologies at order G^4 are three-loop topologies in the worldline picture, namely topologies (d), (f), and (g) in figure 4 (see also figure 12 in [13]). It is Feynman graphs with these topologies that are counted in the relevant entry in table 1. As we shall see below in section 3.4, these are also the graphs that give rise to the novel features that appear in this sector.

3.2 Graphs

We are now ready to enumerate the full set of Feynman graphs that contribute to the $N^3\text{LO}$ spin-orbit sector at G^4 . Clearly, as can also be understood from glancing at table 1, the construction of the current sector builds on the $N^2\text{LO}$ spin-orbit and the non-spinning $N^3\text{LO}$ sectors, with the notable difference that the latter does not introduce three-loop graphs in the worldline picture [36, 37]. This is yet another sense in which the spinning sector is more complicated than the non-spinning sector, because all possible topologies are realized at each order in G , even when the KK field decomposition is used [14, 15, 39]. Further, the presence of a single spin coupling among the worldline insertions means that fewer graphs are equivalent under the permutation of worldline insertions, leading to more unique graphs in the spin-orbit sector than in the non-spinning sectors. In fact, there are far more distinct graphs in the $N^3\text{LO}$ spin-orbit sector at G^4 than even at $N^5\text{LO}$ in the non-spinning sector at G^6 [52, 53].

The generation of the Feynman graphs was carried out using the `FeynGen` module of the `EFTofPNG` public code [16], which was extended to this order. The extension of the code and the graphs were crosschecked. The graphs are drawn (using JaxoDraw [54, 55] based on [56]) in figures 5–11 below. The higher-rank topologies are the more complex, and as such they give rise to the highest numbers of unique graphs. In general, the more self-interaction vertices in a topology, the more graphs it contributes to the sector. All in all, there are 388 unique graphs in the sector; 174 of these are three-loop graphs, and are shown in figures 9–11. 93 of these are higher-rank graphs—in particular, 26 are rank-two, and 67 are rank-three. The higher-rank graphs are reduced using IBP methods, as discussed below. For comparison, in lower-order sectors only 17 rank-two graphs contribute, yet these graphs still constituted the bottleneck of the calculation, even when automated using the first version of the public `EFTofPNG` code. Therefore, it was clear that more advanced integration methods, in particular for the reduction of higher-rank integrals, would be necessary.

3.3 Integration and scalability

To evaluate the graphs in this sector we made use of the public `EFTofPNG` code, with significant upgrades to its `NLoop` and `Main` modules [16].

Higher-rank integrals are reduced using the integration by parts (IBP) method [49], which was previously implemented within the `EFTofPNG` code for rank-two integrals, with

the IBP reduction done ‘by hand’. IBP relations were first applied to two-point graphs with three-loop massless propagators in [57], and the algorithmic reduction was developed in [58, 59]. The main development in the EFTofPNG code involves a new implementation of the algorithmic IBP method.

The upgraded code processes the integrals in this sector in several stages. First, the integrations are streamlined by separating into an external Fourier momentum and three internal loop momenta, similarly to the change of variables used in eqs. (3.2) and (3.3). Next, all tensor dependence in the loop momenta is removed from the numerators via the projection method [60–62], which may be familiar to the readers from the Passarino-Veltman procedure at one-loop [63] (see also [64, 65] for a useful modern presentation of the method). Since spins are derivatively coupled, tensor numerators are present as high as rank eight, similar to the rank encountered at the N⁵LO in the non-spinning sector. Finally, the resulting integrals are reduced using IBP relations [49] via a variant of Laporta’s algorithm [59], resulting in expressions in terms of only three basic scalar integrals, corresponding to the three basic topology types at order G^4 , specified in section 3.1. Altogether, the code runs over approximately two days.

This upgrade will be made publicly available in a future update of the code, and will be presented in a forthcoming publication.

3.4 Findings

The values of the individual Feynman graphs are found in the ancillary files to this publication (both in PDF and in machine-readable files). When two graphs are related by exchange of worldline labels, $1 \leftrightarrow 2$, we present only the graph with spin coupling on worldline “1”. All the new results in this work were confirmed via 2 independent implementations of the formulation and the machinery presented in the previous sections.

Let us point out here some notable features of our results. Of these features, those which are new to the spinning sector arise uniquely from three-loop topologies and thus did not show up at the N³LO non-spinning sector at G^4 within EFT derivations [36, 37, 53].

Zeros. There are a total of 40 graphs that vanish in the present sector. Of these, 25 can be understood due to the presence of contact interaction terms. The nested-factorizable topologies (c1) and (e4) in figure 4 yield zeros due to their dependence on $\epsilon \equiv d - 3$. Such zeros appear at order G^3 , where the factorizable two-loop topologies behave as:

$$\text{Fig. 3(c1),(d1)} \propto [\Gamma(-\epsilon)]^{-1} \sim \epsilon + \mathcal{O}(\epsilon^2). \quad (3.5)$$

At order G^4 the nested-factorizable topologies (c1) and (e4) in figure 4 contain the factorizable two-loop topologies as their subgraphs, and we then have for them:

$$\text{Fig. 4(c1),(e4)} \propto \zeta(2)[\Gamma(-\epsilon)]^{-1} \sim \zeta(2)\epsilon + \mathcal{O}(\epsilon^2), \quad (3.6)$$

which gives rise to the appearance of $\zeta(2) = \pi^2/6$ in rank-three graphs as we discuss below. To recap, graphs of the nested-factorizable topologies, similar to the factorizable two-loop topologies, stand here for purely short-distance contributions, which are contact interaction terms of the form $\delta(\vec{r})$, with $\vec{r} \equiv \vec{r}_1 - \vec{r}_2$ [26].

The remaining 15 graphs are sporadic and vanish due to a variety of miscellaneous reasons.

Riemann zeta values. The rank-three topologies (f5), (g4), and (g5), give rise to terms proportional to $\zeta(2) = \pi^2/6$, and are the source of all transcendental contributions to our result, the first such observed in the spinning sector. We recall that the rank-three topologies involve a linear combination of all three basic three-loop integrals, and that these $\zeta(2)$ factors in particular originate uniquely from the nested-factorizable integral as noted in eq. (3.6) above. Now, we recall that the IBP reduction relations yield linear combinations of basic integrals, with the coefficients including also the factor ϵ^{-1} , i.e. with explicit poles in ϵ , see e.g. [26]. Hence, in these rank-three topologies we have poles canceling out the zeros in ϵ , and the $\zeta(2)$ factor is then uncovered. There are 31 graphs of the three rank-three topologies that give rise to terms that contain $\zeta(2)$.

Riemann zeta values occur in quantum loop corrections starting at one loop, and thus in view of the contact interaction terms, associated with encapsulated UV physics as noted above, that arise at the N^2LO , it is not surprising that such Riemann zeta values appear in the related graphs at N^3LO . Let us point out that topology (e8), which is a rank-two topology, comprised from two of the three basic integrals, also contains the nested-factorizable integral with the $\zeta(2)$ factor, yet it does not yield terms with $\zeta(2)$. This is because topology (e8) is trivially factorized into the rank-two topology (d3) in figure 3, which appears at the N^2LO , where such transcendental numbers do not emerge; Stated differently, topology (e8) is simply a two-loop topology in the worldline picture.

Simple poles and logarithms. Most of the three-loop graphs in the worldline picture (corresponding to graphs with one of the topologies (d), (f), or (g) in figure 4) yield simple poles in $\epsilon \equiv d - 3$ in conjunction with logarithms in r/R_0 . This is because these graphs contain contributions proportional to the factor $\Gamma(\epsilon)(r/R_0)^{-4\epsilon}$, which gives rise to these poles and logarithms upon expansion in ϵ . In this sector all of the aforementioned topologies (except the three nested-nested topologies (d2), (f3), and (g2)) yield such terms, namely both the factorizable-nested and the nested-nested basic types. All in all, 131 of the three-loop graphs give rise to such terms.

Let us highlight again that only the two basic types of factorizable-nested and nested-nested integrals, when they occur within the three-loop topologies in the worldline picture, give rise to poles in ϵ and logarithms, whereas only the nested-factorizable integrals, when contained within three-loop graphs, gives rise to the $\zeta(2)$ factors. Thus, these two behaviors occur entirely independently: there are numerous rank-one three-loop graphs with poles and logarithms and no $\zeta(2)$ factors, and conversely the rank-three graph (g5.1) in figure 11, which yields a $\zeta(2)$ factor, does not involve any poles or logarithms.

4 N³LO gravitational spin-orbit action at G^4

Adding up all of the graphs we get the following contribution to the N³LO spin-orbit Lagrangian at G^4 :

$$L_{\text{SO}}^{\text{N}^3\text{LO}} = \frac{G^4}{r^5} \frac{\vec{S}_1}{m_1} \cdot \vec{v} \times \vec{n} \left[\left(\frac{20}{3} - 13\zeta(2) - \frac{5}{3} \left(\frac{1}{\epsilon} - 4 \log(r/R_0) \right) \right) m_1^3 m_2^2 - \frac{31}{3} m_1^2 m_2^3 \right. \\ \left. - \frac{3}{8} m_1 m_2^4 \right] + [1 \leftrightarrow 2], \quad (4.1)$$

where $\epsilon_{ijk} S_k = S_{ij}$, with ϵ_{ijk} the 3-dimensional Levi-Civita symbol, $\vec{v} \equiv \vec{v}_1 - \vec{v}_2$, and $\vec{n} \equiv \vec{r}/r$. Note the overall dependence only on the relative velocity, \vec{v} , rather than on each of the worldline velocities separately, similar to the total results from topologies at the highest order in G at lower PN orders in the spin-orbit sector [28, 40].

Notice that all the contributions proportional to $m_1^3 m_2$ conspire to cancel out from the total result, though they appear in many topologies and individual graphs' values. This vanishing coefficient would have been the leading contribution in the test-particle limit, where the extreme-mass-ratio limit holds, i.e. $m_1 \gg m_2$, and the body “2” can be considered as a test particle moving in the Kerr metric (in harmonic coordinates) generated by body “1”.

Interestingly, the poles, logarithms, and factors of $\zeta(2)$ eventually appear only in the term proportional to $m_1^2 m_2^2$. Note that the appearance of these features in the total result differs from the situation in the non-spinning sector within EFT derivations, where all the poles in ϵ , logarithms, and Riemann zeta values, which show up in general as of the N³LO, conspire to cancel out in each of the N ^{n} LO sectors at G^{n+1} for $n \leq 5$, so that they all contain only finite terms with only rational coefficients [53].

5 Conclusions

In this paper we have computed for the first time the contribution to the N³LO gravitational spin-orbit coupling from interaction at G^4 via the EFT of spinning gravitating objects [18]. The computation is carried out in terms of Feynman diagrams with topologies at this order (see figure 4), and relied on extending and developing the `EFTofPNG` public code [16]. This constitutes the most computationally challenging part of the N³LO spin-orbit sector, as far as integration is concerned, because it contains all possible topologies at G^4 , including three-loop level. This sector enters at the 4.5PN order for maximally-rotating compact objects, and completes the results of [22] at this order, thus pushing the current state of the art to the 4.5PN accuracy.

The N³LO spin-orbit coupling at G^4 consists of 388 distinct graphs to evaluate. Of these graphs 174 are genuine three-loop graphs in the worldline picture, which give rise to new special features in the spinning sector, that also show up in the final result of the topologies at this order. These features include simple poles and logarithms that arise from dimensional regularization, as well as the appearance of transcendental factors, which

can be understood as next-order corrections of purely short-distance contributions that vanish in the classical context. This is in contrast to the non-spinning sector within EFT computations, where such special features conspire to cancel out from the final result in each of the $N^n\text{LO}$ sectors at G^{n+1} for $n \leq 5$.

We provide here a comprehensive account of the topologies in the worldline picture of the EFT approach. Further, all the computational aspects of the work are carried out via the unique **EFTofPNG** code. Due to the increased intricacy of this sector we have developed the **EFTofPNG** code, incorporating further techniques from the realm of particle amplitudes. We expect these developments to be extremely useful for studies of PN gravity, and we plan to release a public update to the **EFTofPNG** code to be presented in a forthcoming publication. The present sector illustrates once again that not only is tackling spins in gravity conceptually challenging, it is also more computationally challenging, as the higher conceptual intricacy is also reflected at the computational level in various aspects of the calculations.

To complete the $N^3\text{LO}$ spin-orbit sector all of the remaining contributions from topologies at up to order G^3 should also be evaluated. Of the latter, the contribution at G^3 is the most computationally demanding as it is the only remaining one with higher-rank graphs that require reduction, on top of the large number of contributing graphs. Nonetheless, we believe that our extensions of the **EFTofPNG** code are well-suited to handle this challenge. In general, lower orders in G are challenging due to the higher-order spin couplings and the proliferation of time derivatives. These contributions from lower orders in G will also fix the resolution of the simple pole and logarithm that are left in the total result here. Thus, the completion of the $N^3\text{LO}$ spin-orbit at all orders in G will be reported in forthcoming publications.

Finally, it is evident that such high-precision computations require crosschecks, preferably via independent PN methodologies. Therefore, prospective studies that overlap with these sectors, possibly incorporating further modern amplitudes methods as in [66–70], are extremely desirable.

Acknowledgments

ML receives funding from the European Union’s Horizon 2020 research and innovation programme under the Marie Skłodowska Curie grant agreements No. 847523 and No. 764850, and from the Carlsberg Foundation. ML has also been supported by the European Union’s Horizon 2020 Framework Programme FP8/2014-2020 “preQFT” starting grant No. 639729. ML is grateful to Freddy Cachazo for the warm hospitality at Perimeter Institute where the final stages of this work were carried out. AJM and MvH are both supported by an ERC starting grant No. 757978 and a grant from the Villum Fonden No. 15369. AJM is also supported by a Carlsberg Postdoctoral Fellowship (CF18-0641). MvH is also supported by the European Union’s Horizon 2020 research and innovation programme under grant agreement No. 793151.

References

- [1] “LIGO webpage.” <http://www.ligo.caltech.edu>.
- [2] LIGO, VIRGO collaboration, B. P. Abbott et al., *Observation of Gravitational Waves from a Binary Black Hole Merger*, *Phys. Rev. Lett.* **116** (2016) 061102 [[1602.03837](#)].
- [3] “Virgo webpage.” <http://www.virgo-gw.eu>.
- [4] “KAGRA webpage.” <http://gwcenter.icrr.u-tokyo.ac.jp/en>.
- [5] “IndiGO webpage.” <http://www.gw-indigo.org>.
- [6] M. Punturo et al., *The Einstein Telescope: A third-generation gravitational wave observatory*, *Class. Quant. Grav.* **27** (2010) 194002.
- [7] KOREAN GRAVITATIONAL WAVE GROUP collaboration, H. J. Paik, H. M. Lee, K. Cho and J. Kim, *Gravitational-wave Detectors and a New Low-frequency Detector SOGRO*, *New Phys. Sae Mulli* **66** (2016) 272.
- [8] “ESA LISA webpage.” <http://sci.esa.int/lisa>.
- [9] TIANQIN collaboration, J. Luo et al., *TianQin: a space-borne gravitational wave detector*, *Class. Quant. Grav.* **33** (2016) 035010 [[1512.02076](#)].
- [10] L. Blanchet, *Gravitational Radiation from Post-Newtonian Sources and Inspiralling Compact Binaries*, *Living Rev. Rel.* **17** (2014) 2 [[1310.1528](#)].
- [11] A. Buonanno and T. Damour, *Effective one-body approach to general relativistic two-body dynamics*, *Phys.Rev.* **D59** (1999) 084006 [[gr-qc/9811091](#)].
- [12] W. D. Goldberger and I. Z. Rothstein, *An Effective field theory of gravity for extended objects*, *Phys.Rev.* **D73** (2006) 104029 [[hep-th/0409156](#)].
- [13] M. Levi, *Effective Field Theories of Post-Newtonian Gravity: A comprehensive review*, *Rept. Prog. Phys.* **83** (2020) 075901 [[1807.01699](#)].
- [14] B. Kol and M. Smolkin, *Non-Relativistic Gravitation: From Newton to Einstein and Back*, *Class.Quant.Grav.* **25** (2008) 145011 [[0712.4116](#)].
- [15] B. Kol, M. Levi and M. Smolkin, *Comparing space+time decompositions in the post-Newtonian limit*, *Class.Quant.Grav.* **28** (2011) 145021 [[1011.6024](#)].
- [16] M. Levi and J. Steinhoff, *EFTofPNG: A package for high precision computation with the Effective Field Theory of Post-Newtonian Gravity*, *Class. Quant. Grav.* **34** (2017) 244001 [[1705.06309](#)].
- [17] M. Levi, *A public framework for Feynman calculations and post-Newtonian gravity*, [1811.12401](#).
- [18] M. Levi and J. Steinhoff, *Spinning gravitating objects in the effective field theory in the post-Newtonian scheme*, *JHEP* **09** (2015) 219 [[1501.04956](#)].
- [19] M. Levi and J. Steinhoff, *Leading order finite size effects with spins for inspiralling compact binaries*, *JHEP* **06** (2015) 059 [[1410.2601](#)].
- [20] M. Levi and J. Steinhoff, *Next-to-next-to-leading order gravitational spin-squared potential via the effective field theory for spinning objects in the post-Newtonian scheme*, *JCAP* **1601** (2016) 008 [[1506.05794](#)].

- [21] M. Levi and J. Steinhoff, *Complete conservative dynamics for inspiralling compact binaries with spins at fourth post-Newtonian order*, [1607.04252](#).
- [22] M. Levi, S. Mougiakakos and M. Vieira, *Gravitational cubic-in-spin interaction at the next-to-leading post-Newtonian order*, *JHEP* **01** (2021) 036 [[1912.06276](#)].
- [23] M. Levi, A. J. McLeod and M. von Hippel, *NNLO gravitational quadratic-in-spin interactions at the quartic order in G* , *JHEP* **07** (2021) 116 [[2003.07890](#)].
- [24] M. Levi and F. Teng, *NLO gravitational quartic-in-spin interaction*, *JHEP* **01** (2021) 066 [[2008.12280](#)].
- [25] N. Arkani-Hamed, T.-C. Huang and Y.-t. Huang, *Scattering Amplitudes For All Masses and Spins*, [1709.04891](#).
- [26] M. Levi, *Binary dynamics from spin1-spin2 coupling at fourth post-Newtonian order*, *Phys.Rev.* **D85** (2012) 064043 [[1107.4322](#)].
- [27] M. Levi and J. Steinhoff, *Equivalence of ADM Hamiltonian and Effective Field Theory approaches at next-to-next-to-leading order spin1-spin2 coupling of binary inspirals*, *JCAP* **1412** (2014) 003 [[1408.5762](#)].
- [28] M. Levi and J. Steinhoff, *Next-to-next-to-leading order gravitational spin-orbit coupling via the effective field theory for spinning objects in the post-Newtonian scheme*, *JCAP* **1601** (2016) 011 [[1506.05056](#)].
- [29] P. Jaranowski and G. Schäfer, *Third postNewtonian higher order ADM Hamilton dynamics for two-body point mass systems*, *Phys.Rev.* **D57** (1998) 7274 [[gr-qc/9712075](#)].
- [30] P. Jaranowski and G. Schäfer, *The Binary black hole problem at the third postNewtonian approximation in the orbital motion: Static part*, *Phys. Rev.* **D60** (1999) 124003 [[gr-qc/9906092](#)].
- [31] L. Blanchet and G. Faye, *Equations of motion of point particle binaries at the third postNewtonian order*, *Phys. Lett.* **A271** (2000) 58 [[gr-qc/0004009](#)].
- [32] L. Blanchet and G. Faye, *General relativistic dynamics of compact binaries at the third postNewtonian order*, *Phys. Rev.* **D63** (2001) 062005 [[gr-qc/0007051](#)].
- [33] T. Damour, P. Jaranowski and G. Schäfer, *Dimensional regularization of the gravitational interaction of point masses*, *Phys. Lett.* **B513** (2001) 147 [[gr-qc/0105038](#)].
- [34] Y. Itoh and T. Futamase, *New derivation of a third postNewtonian equation of motion for relativistic compact binaries without ambiguity*, *Phys. Rev.* **D68** (2003) 121501 [[gr-qc/0310028](#)].
- [35] L. Blanchet, T. Damour and G. Esposito-Farese, *Dimensional regularization of the third postNewtonian dynamics of point particles in harmonic coordinates*, *Phys. Rev.* **D69** (2004) 124007 [[gr-qc/0311052](#)].
- [36] M. Levi, *Binary dynamics at third post-Newtonian order via an effective field theory approach*, *unpublished* (2011) .
- [37] S. Foffa and R. Sturani, *Effective field theory calculation of conservative binary dynamics at third post-Newtonian order*, *Phys.Rev.* **D84** (2011) 044031 [[1104.1122](#)].
- [38] L. Blanchet, A. Buonanno and G. Faye, *Tail-induced spin-orbit effect in the gravitational radiation of compact binaries*, *Phys.Rev.* **D84** (2011) 064041 [[1104.5659](#)].

- [39] M. Levi, *Next to Leading Order gravitational Spin1-Spin2 coupling with Kaluza-Klein reduction*, *Phys.Rev.* **D82** (2010) 064029 [[0802.1508](#)].
- [40] M. Levi, *Next to Leading Order gravitational Spin-Orbit coupling in an Effective Field Theory approach*, *Phys.Rev.* **D82** (2010) 104004 [[1006.4139](#)].
- [41] M. E. Peskin and D. V. Schroeder, *An Introduction to quantum field theory*. Addison-Wesley, Reading, USA, 1995.
- [42] B. Kol and M. Smolkin, *Einstein's action and the harmonic gauge in terms of Newtonian fields*, *Phys.Rev.* **D85** (2012) 044029 [[1009.1876](#)].
- [43] A. J. Hanson and T. Regge, *The Relativistic Spherical Top*, *Annals Phys.* **87** (1974) 498.
- [44] I. Bailey and W. Israel, *Lagrangian Dynamics of Spinning Particles and Polarized Media in General Relativity*, *Commun.Math.Phys.* **42** (1975) 65.
- [45] R. A. Porto, *Post-Newtonian corrections to the motion of spinning bodies in NRGR*, *Phys.Rev.* **D73** (2006) 104031 [[gr-qc/0511061](#)].
- [46] J. Hartung and J. Steinhoff, *Next-to-next-to-leading order post-Newtonian spin-orbit Hamiltonian for self-gravitating binaries*, *Annalen Phys.* **523** (2011) 783 [[1104.3079](#)].
- [47] S. Marsat, A. Bohé, G. Faye and L. Blanchet, *Next-to-next-to-leading order spin-orbit effects in the equations of motion of compact binary systems*, *Class.Quant.Grav.* **30** (2013) 055007 [[1210.4143](#)].
- [48] A. Bohé, S. Marsat, G. Faye and L. Blanchet, *Next-to-next-to-leading order spin-orbit effects in the near-zone metric and precession equations of compact binaries*, *Class.Quant.Grav.* **30** (2013) 075017 [[1212.5520](#)].
- [49] V. A. Smirnov, *Feynman integral calculus*. Springer, Berlin, Germany, 2006.
- [50] B. Kol and R. Shir, *Classical 3-loop 2-body diagrams*, *JHEP* **09** (2013) 069 [[1306.3220](#)].
- [51] S. Foffa and R. Sturani, *Conservative dynamics of binary systems to fourth Post-Newtonian order in the EFT approach I: Regularized Lagrangian*, *Phys. Rev.* **D100** (2019) 024047 [[1903.05113](#)].
- [52] S. Foffa, P. Mastrolia, R. Sturani, C. Sturm and W. J. Torres Bobadilla, *Static two-body potential at fifth post-Newtonian order*, *Phys. Rev. Lett.* **122** (2019) 241605 [[1902.10571](#)].
- [53] J. Blümlein, A. Maier and P. Marquard, *Five-Loop Static Contribution to the Gravitational Interaction Potential of Two Point Masses*, *Phys. Lett.* **B800** (2020) 135100 [[1902.11180](#)].
- [54] D. Binosi and L. Theussl, *JaxoDraw: A Graphical user interface for drawing Feynman diagrams*, *Comput. Phys. Commun.* **161** (2004) 76 [[hep-ph/0309015](#)].
- [55] D. Binosi, J. Collins, C. Kaufhold and L. Theussl, *JaxoDraw: A Graphical user interface for drawing Feynman diagrams. Version 2.0 release notes*, *Comput. Phys. Commun.* **180** (2009) 1709 [[0811.4113](#)].
- [56] J. A. M. Vermaseren, *Axodraw*, *Comput. Phys. Commun.* **83** (1994) 45.
- [57] K. G. Chetyrkin and F. V. Tkachov, *Integration by Parts: The Algorithm to Calculate beta Functions in 4 Loops*, *Nucl. Phys.* **B192** (1981) 159.
- [58] S. Laporta and E. Remiddi, *The Analytical value of the electron (g-2) at order alpha**3 in QED*, *Phys. Lett.* **B379** (1996) 283 [[hep-ph/9602417](#)].

- [59] S. Laporta, *High precision calculation of multiloop Feynman integrals by difference equations*, *Int. J. Mod. Phys. A* **15** (2000) 5087 [[hep-ph/0102033](#)].
- [60] R. Karplus and M. Neuman, *Non-Linear Interactions between Electromagnetic Fields*, *Phys. Rev.* **80** (1950) 380.
- [61] B. A. Kniehl, *Associated Production of Higgs and Z Bosons From Gluon Fusion in Hadron Collisions*, *Phys. Rev.* **D42** (1990) 2253.
- [62] T. Binoth, E. W. N. Glover, P. Marquard and J. J. van der Bij, *Two loop corrections to light by light scattering in supersymmetric QED*, *JHEP* **05** (2002) 060 [[hep-ph/0202266](#)].
- [63] G. Passarino and M. J. G. Veltman, *One Loop Corrections for $e^+ e^-$ Annihilation Into $\mu^+ \mu^-$ in the Weinberg Model*, *Nucl. Phys.* **B160** (1979) 151.
- [64] R. H. Boels, Q. Jin and H. Luo, *Efficient integrand reduction for particles with spin*, [1802.06761](#).
- [65] L. Chen, *A prescription for projectors to compute helicity amplitudes in D dimensions*, [1904.00705](#).
- [66] F. Cachazo and A. Guevara, *Leading Singularities and Classical Gravitational Scattering*, *JHEP* **02** (2020) 181 [[1705.10262](#)].
- [67] A. Guevara, *Holomorphic Classical Limit for Spin Effects in Gravitational and Electromagnetic Scattering*, *JHEP* **04** (2019) 033 [[1706.02314](#)].
- [68] C. Cheung, I. Z. Rothstein and M. P. Solon, *From Scattering Amplitudes to Classical Potentials in the Post-Minkowskian Expansion*, *Phys. Rev. Lett.* **121** (2018) 251101 [[1808.02489](#)].
- [69] Z. Bern, C. Cheung, R. Roiban, C.-H. Shen, M. P. Solon and M. Zeng, *Scattering Amplitudes and the Conservative Hamiltonian for Binary Systems at Third Post-Minkowskian Order*, *Phys. Rev. Lett.* **122** (2019) 201603 [[1901.04424](#)].
- [70] Z. Bern, C. Cheung, R. Roiban, C.-H. Shen, M. P. Solon and M. Zeng, *Black Hole Binary Dynamics from the Double Copy and Effective Theory*, *JHEP* **10** (2019) 206 [[1908.01493](#)].

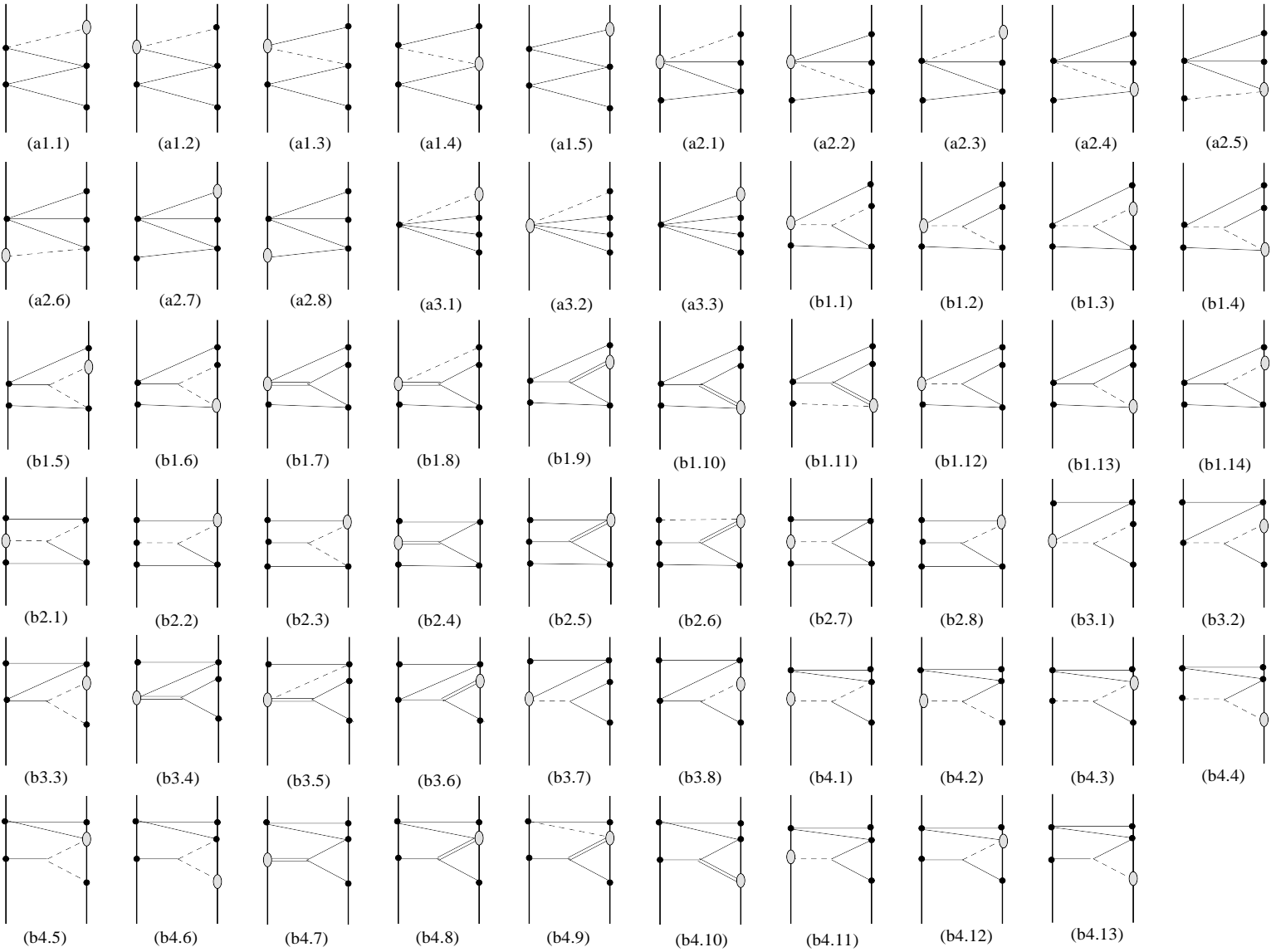


Figure 5. Feynman graphs which contribute to the $N^3\text{LO}$ spin-orbit coupling at G^4 . This figure contains all graphs with topologies (a) and (b1)-(b4) of figure 4. All of the graphs presented in this figure and the following ones should be accompanied by their ‘mirror’ graphs, in which the worldline labels are exchanged, i.e. $1 \leftrightarrow 2$.

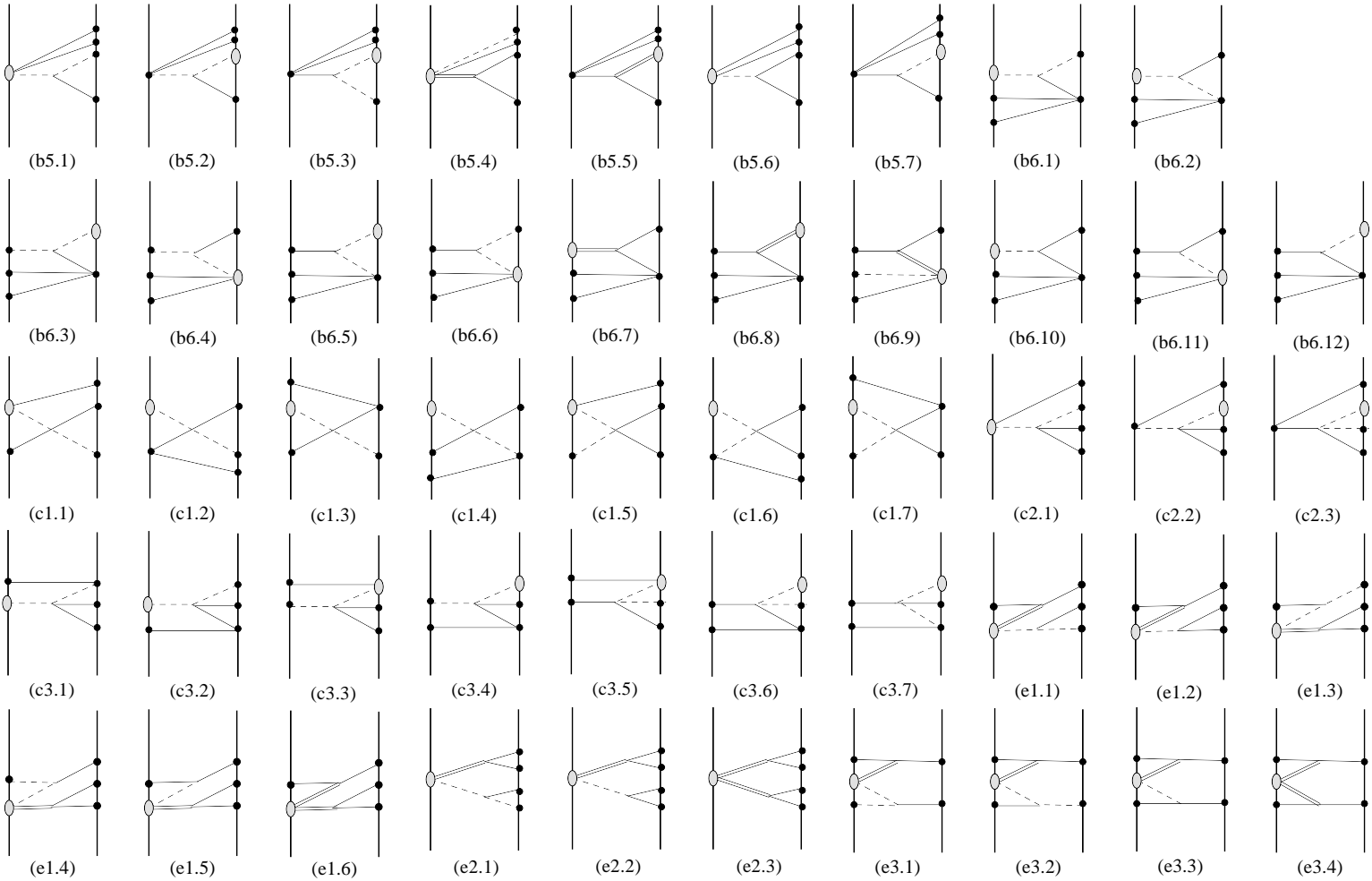


Figure 6. Feynman graphs which contribute to the $N^3\text{LO}$ spin-orbit coupling at G^4 . This figure contains all graphs with topologies (b5), (b6), (c), and (e1)-(e3), of figure 4.

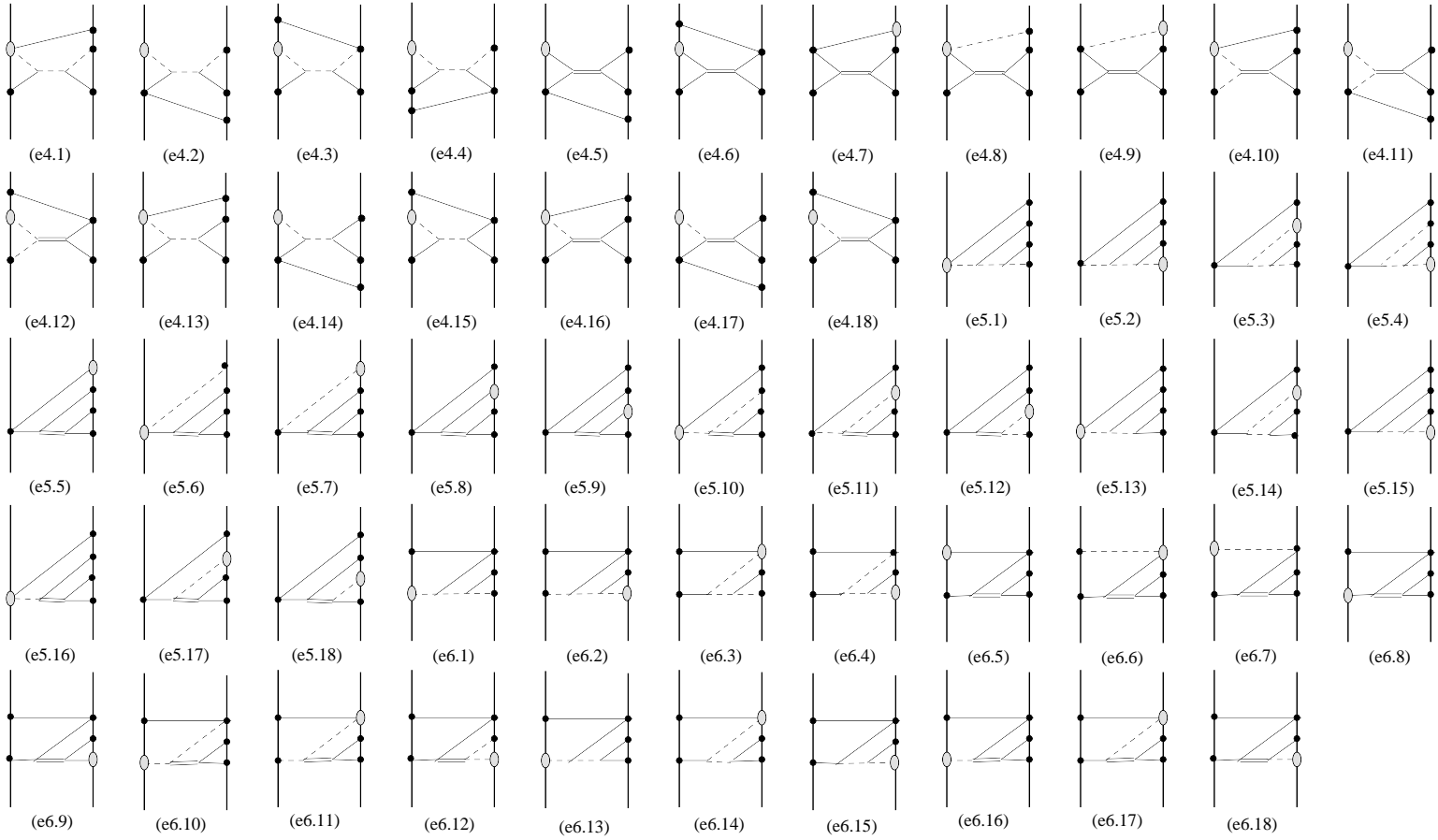


Figure 7. Feynman graphs which contribute to the $N^3\text{LO}$ spin-orbit coupling at G^4 . This figure contains all graphs with topologies (e4)-(e6) of figure 4.

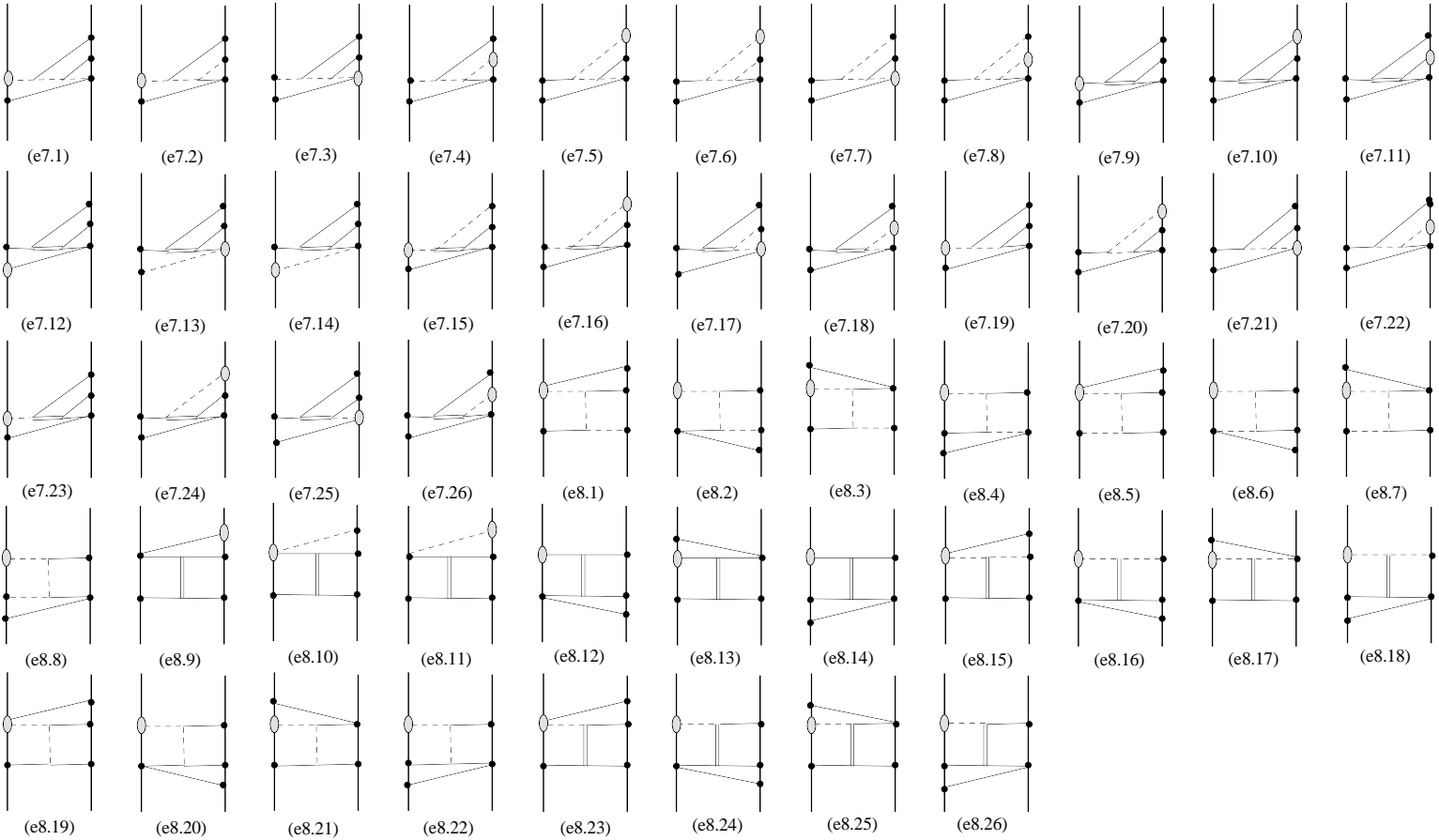


Figure 8. Feynman graphs which contribute to the $N^3\text{LO}$ spin-orbit coupling at G^4 . This figure contains all graphs with topologies (e7) and (e8) of figure 4. The graphs in group (e8) are rank-two graphs, which clearly factorize into the single rank-two topology (d3) in figure 3.

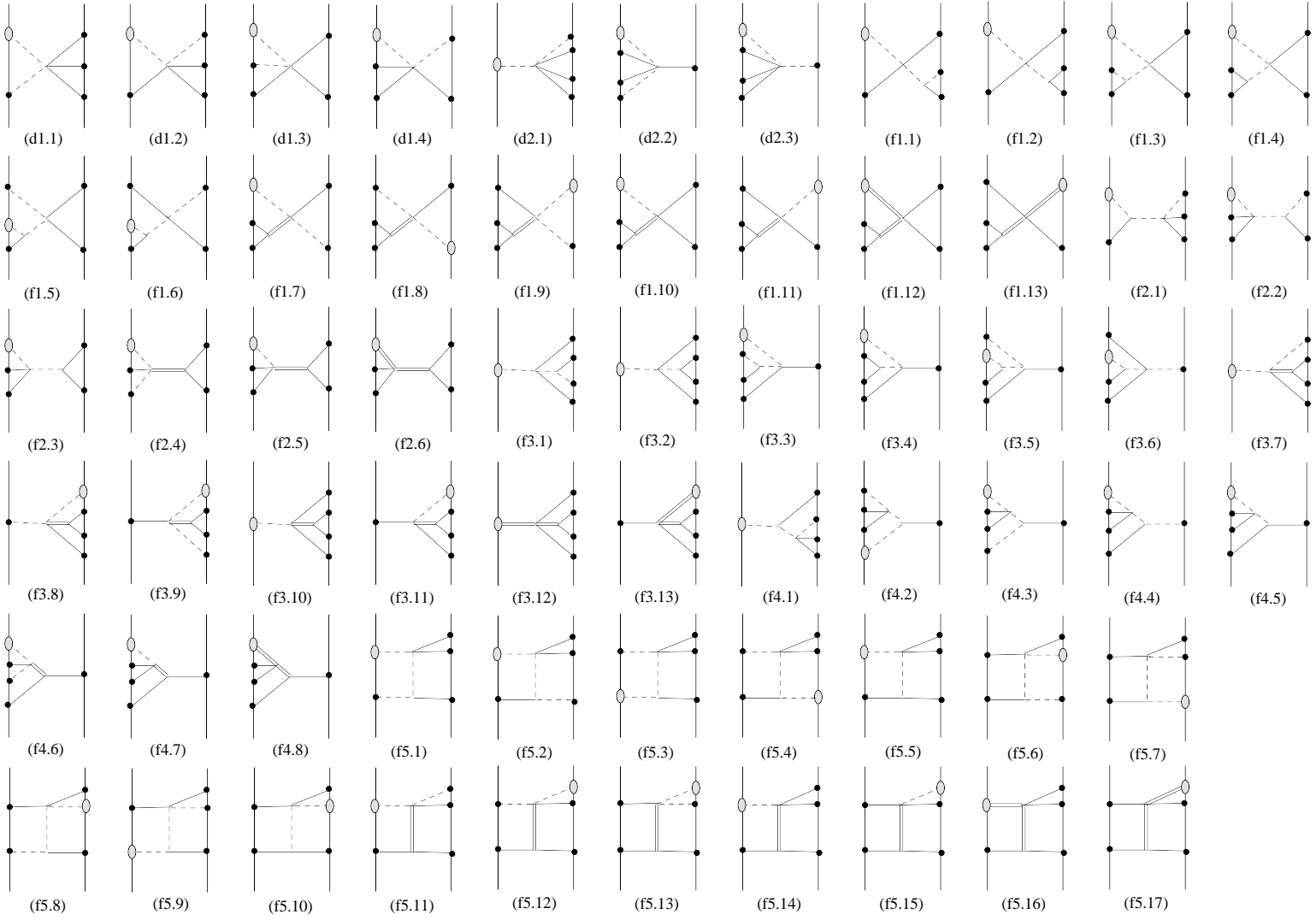


Figure 9. Feynman graphs which contribute to the $N^3\text{LO}$ spin-orbit coupling at G^4 . This figure contains all graphs with topologies (d) and (f) of figure 4. The graphs in group (f5) are rank-three graphs that require reduction, and appear in the non-spinning sector only at $N^4\text{LO}$.

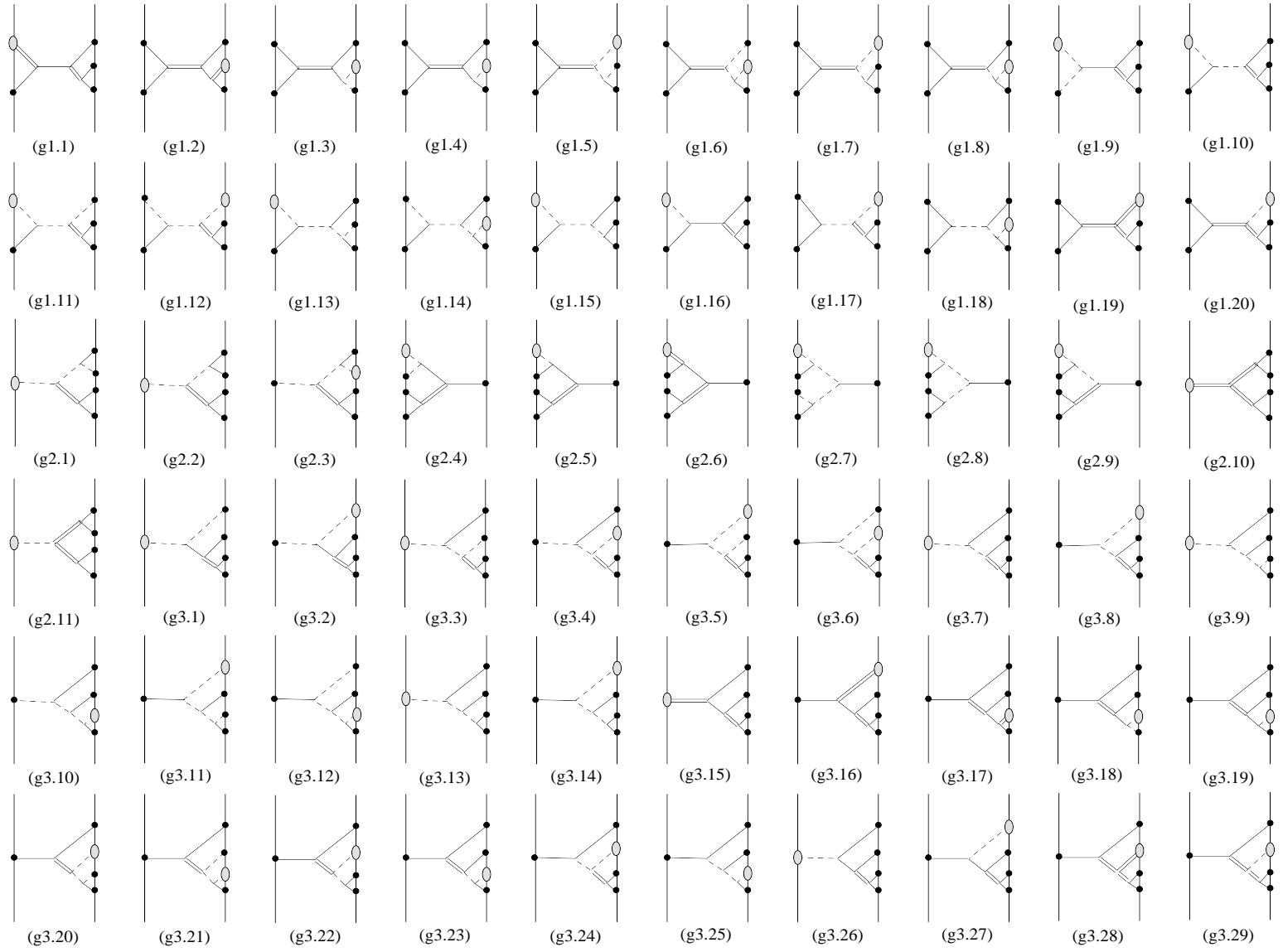


Figure 10. Feynman graphs which contribute to the N^3LO spin-orbit coupling at G^4 . This figure contains all graphs with topologies (g1)-(g3) of figure 4.

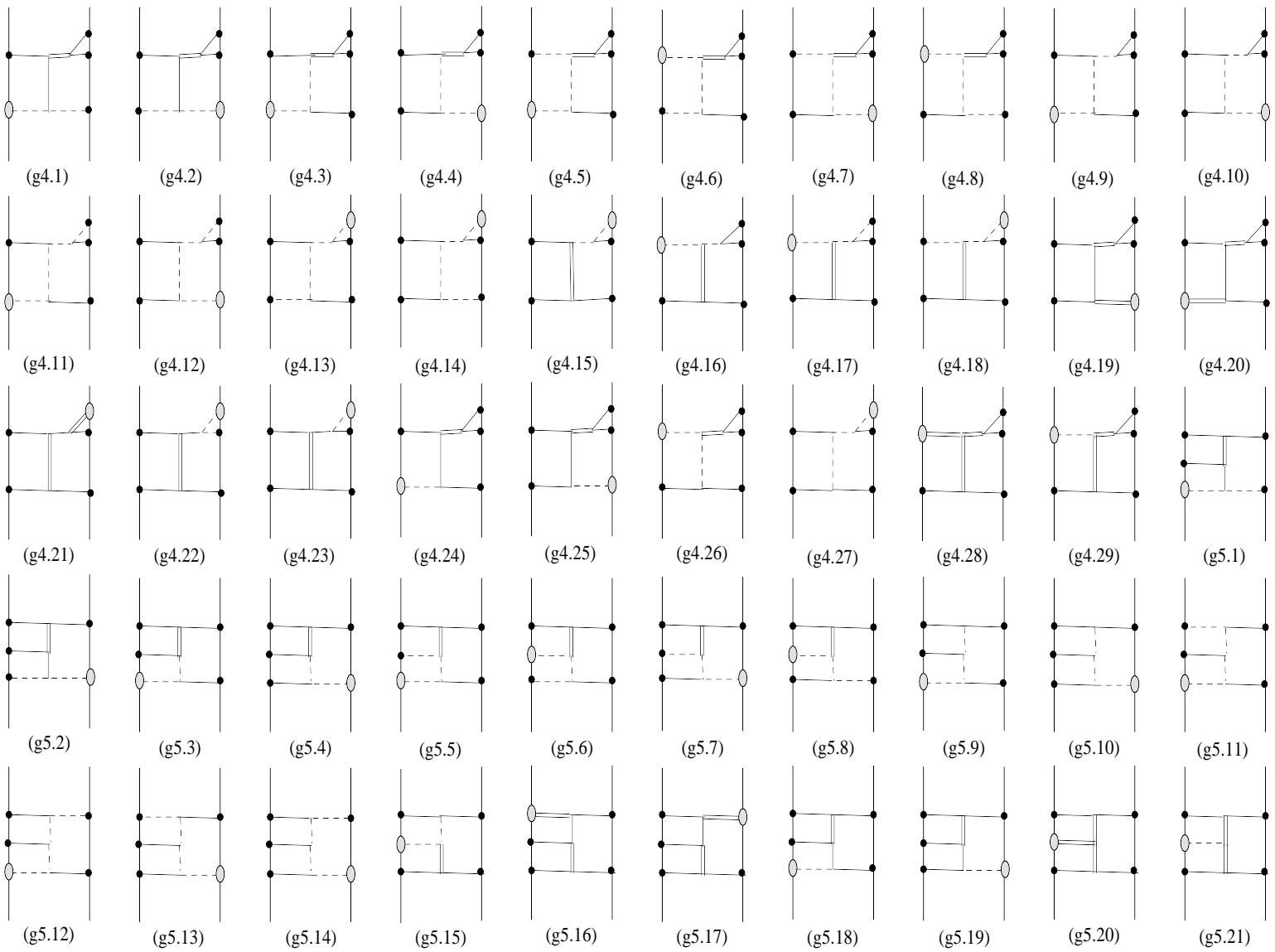


Figure 11. Feynman graphs which contribute to the $N^3\text{LO}$ spin-orbit coupling at G^4 . This figure contains all graphs with topologies (g^4) - (g^5) of figure 4. These are rank-three topologies that are deferred in the non-spinning sector to the $N^4\text{LO}$.